Glassy dynamics in CuMn thin-film multilayers

Qiang Zhai,[1,*] David C. Harrison,[2] Daniel Tennant,[1] E. Dan Dahlberg,[2] Gregory G. Kenning,[3] and Raymond L. Orbach[1,†]

[1]*Texas Materials Institute, The University of Texas at Austin, Austin, Texas 78712, USA*

[2]*School of Physics and Astronomy, The University of Minnesota, Minneapolis, Minnesota 55455, USA*

[3]*Department of Physics, Indiana University of Pennsylvania, Indiana, Pennsylvania 15705, USA*

(Received 4 December 2016; published 6 February 2017; corrected 8 April 2019)

Thin-film multilayered spin-glass CuMn/Cu structures display glassy dynamics. The freezing temperature T_f was measured for 40 layers of CuMn films of thickness $\mathcal{L} = 4.5$,9.0, and 20.0 nm, sandwiched between nonmagnetic Cu layers of thickness ≈60 nm. The Kenning effect, $T_f \propto \ln \mathcal{L}$, is shown to follow from power-law dynamics where the correlation length grows from nucleation as $\xi(t,T) = c_1 a_0 (t/\tau_0)^{c_2(T/T_g)}$, leading to $[(T_f/T_g)c_2 \ln(t_{co}/\tau_0)] + \ln c_1 = \ln(\mathcal{L}/a_0)$. Here, T_g is the bulk spin-glass temperature, c_1 and c_2 are constants determined from the spin-glass dynamics, t_{co} is the time for the correlation length to grow to the film thickness, τ_0 is a characteristic exchange time $\approx \hbar/k_B T_g$, and a_0 is the average Mn-Mn separation. For $t \geqslant t_{co}$, the magnetization dynamics are simple activated, with a single activation energy $\Delta_{max}(\mathcal{L})/k_B T_g = (1/c_2)[\ln(\mathcal{L}/a_0) - \ln c_1]$ that does not change with time. Values for all these parameters are found for the three values of $\mathcal{L}$ explored in these measurements. We find experimentally $\Delta_{max}(\mathcal{L})/k_B = 907$, 1246, and 1650 K, respectively, for the three CuMn thin-film multilayer thicknesses, consistent with power-law dynamics. We perform a similar analysis based on the activated dynamics of the droplet model and find a much larger spread for $\Delta_{max}(\mathcal{L})$ than found experimentally.

DOI: 10.1103/PhysRevB.95.054304

I. INTRODUCTION

The dynamical properties of spin glasses are strongly dependent on dimension, with recent interest in the "mesoscopic" regime [1], defined by length scales $\mathcal{L}$ less than 50 nm. For example, recent experiments [2,3] on $Ge_{89}Mn_{11}$, with $\mathcal{L} =$ 15.5 nm, have displayed dimensional crossover from $D = 3$ to $D = 2$ as a function of time and temperature. This crossover occurs because the time-dependent (t) and temperature-dependent (T) spin-glass correlation length $\xi(t,T)$ grows from nucleation at $t = 0$ to $\mathcal{L}$ at a time designated as t_{co}. At $\xi(t_{co},T) = \mathcal{L}$, the spin glass becomes two-dimensional for $t \geqslant t_{co}$. Because the lower critical dimension for spin glasses is $D \cong 2.5$ [4,5], this leads to a spin-glass transition temperature $T_g = 0$. This means that there is no further growth of $\xi(t,T)$ in either the perpendicular or parallel directions if the temperature is fixed. The remaining spin-glass correlations for length scales less than order $\mathcal{L}$ represent an excellent "laboratory" for exploration of dynamical properties at fixed length scales.

Experimentally, one observes a time-dependent "freezing" temperature T_f in mesoscopic thin-film spin glasses below which irreversible behavior is exhibited. In this sense, the mesoscopic spin glass behaves as a conventional glass, where the value of T_f depends upon the observation time. We shall show this explicitly with our experimental values of T_f for the different values of $\mathcal{L}$ we investigated ($\mathcal{L} = 4.5$,9.0, and 20 nm) for $Cu_{0.883}Mn_{0.117}$.

There are two competing theories for spin-glass dynamics, one based on Parisi's mean-field solution [6] of the Sherrington-Kirkpatrick infinite-range spin-glass Hamiltonian [7] and the other on the "droplet" model developed by Fisher and Huse [8–12] "motivated by the results of the numerical 'domain-wall' renormalization-group studies" [8,13,14]. The former assumes power-law dynamics for the growth of $\xi(t,T)$, while the latter assumes activated dynamics for the growth of $\xi(t,T)$. Although the two approaches are fundamentally different physical pictures, it has been very difficult to distinguish either experimentally or numerically between the two. Some attempts are given in Refs. [15–18]. The experiments detailed in our paper distinguish between these two approaches by direct measurement of a microscopic parameter, the system's maximum barrier height $\Delta_{max}(\mathcal{L})$, when $\xi(t > t_{co},T)$ is fixed at $\mathcal{L}$. Before going into more detail, it is important to outline the analysis utilized in this paper.

When the spin-glass correlation length $\xi(t,T)$ has reached $\mathcal{L}$ at a time t_{co}, the crossover time, $D = 3$ spin-glass correlations remain for length scales $\leqslant \mathcal{L}$ and generate dynamical spin-glass behavior. When $t > t_{co}$, any property dependent on $\xi(t,T)$ is fixed at the value it has at t_{co}. A particular consequence is that the dynamics follow a simple Arrhenius law, with a single activation energy $\Delta_{max}(\mathcal{L})$ that does not change with time. The two approaches referred to above for the value of $\Delta_{max}(\mathcal{L})$ are both scaled by the bulk spin-glass transition temperature T_g but differ on the dependence of $\Delta_{max}(\mathcal{L})$ on $\mathcal{L}$. Beyond their theoretical differences (and there are many), there is also the prediction that the presence of a magnetic field H will destroy the spin-glass state in the Fisher-Huse droplet model [6], while the Parisi approach leads to a $T_g(H,T)$ as predicted by de Almeida and Thouless [19].

The next section is a brief review of the experimental background for mesoscale spin-glass dynamics. Section III introduces explicit forms for $\xi(t,T)$ for the two different physical models and provides a derivation of the expressions for $\Delta_{max}(\mathcal{L})$ for each. In Sec. IV we present the multilayer sample preparation and the measurement protocols. The measurement protocols are different from those applied to bulk spin glasses because of what we shall show are time-dependent freezing temperatures and hence glassy dynamics for mesoscopic spin glasses. Section V contains the experimental results for both the $\mathcal{L}$-dependent freezing temperatures and activation energies. The analysis and comparison with the two models

*qiang@utexas.edu

†orbach@austin.utexas.edu

 ©2017 American Physical Society

for spin-glass dynamics discussed above comprise Sec. VI. Our results are summarized in Sec. VII.

II. EXPERIMENTAL BACKGROUND FOR THIN-FILM SPIN GLASSES

The first research to address either finite scaling or the crossover from three-dimensional to two-dimensional behavior in long-range Ruderman-Kittel-Kasuya-Yosida (RKKY) spin glasses, after initial reports [20], was that of Kenning *et al.* [21]. In their landmark paper, they took note of the reduction in the freezing temperature T_f with decreasing spin-glass thickness in multilayer samples of $Cu_{1-x}Mn_x$/Cu. They determined T_f by plotting the zero-field-cooled susceptibility $\chi_{ZFC}(T)$ and the field-cooled susceptibility $\chi_{FC}(T)$ as functions of temperature. For $D = 3$ spin glasses, the two are equal for temperatures above the spin-glass transition temperature T_g. Below T_g, the two differ from each other, signaling irreversibility setting in at T_g. For mesoscopic spin glasses, an analogous separation occurs, but at a freezing temperature $T_f < T_g$.

The irreversible magnetization, $M_{FC}(T) - M_{ZFC}(T)$, increases as the temperature is lowered. For thin-film spin glasses, the onset of irreversibility with decreasing temperature is both thickness and time dependent. Representative plots of $M_{FC}(T)$ and $M_{ZFC}(T)$ vs temperature T for the three thicknesses investigated in our work ($\mathcal{L} = 4.5$,9.0, and 20.0 nm), are exhibited in Fig. 1. Similar findings were shown in Fig. 14 of Ref. [21]. They listed values for T_f in their Table VII for their range of $\mathcal{L}$ at each of their three concentrations for their CuMn/Cu multilayers. Their Fig. 21 plotted the ratio T_f/T_g as a function of $\ln \mathcal{L}$. We display their results in Fig. 2, but with $\mathcal{L}$ divided by the relevant average Mn-Mn separation a_0 (we estimate $a_0 = 0.523$ nm for the CuMn concentration in our films; see below). It is seen that T_f/T_g rises roughly linearly with increasing $\ln(\mathcal{L}/a_0)$ out to about $\mathcal{L}/a_0 \approx 5$, beyond which it flattens off to the bulk value T_g.

Figure 2 represents the first systematic study of the freezing temperature T_f differing from the spin-glass transition temperature T_g as a function of diminishing length scale $\ln \mathcal{L}$, which is termed the Kenning effect. We shall show in Sec. VII that it represents "glassy dynamics" in that T_f will be a function of the time scale of the experiment. This is based on the assumption that the correlation length $\xi(t,T)$ has reached the film thickness $\mathcal{L}$, so that there will be activated dynamics with an activation energy $\Delta_{max}(\mathcal{L})$. The freezing temperature T_f is then set by the approximate time scale $\tau_0 \exp[\Delta_{max}(\mathcal{L})/k_B T_f]$, where $1/\tau_0$ is an exchange rate $\sim k_B T_g/\hbar \approx 6.9 \times 10^{12}$ s^{-1} for $T_g \approx 53$ K from measurements of our thick-film samples. As $\mathcal{L}$ increases, the correlation length $\xi(t,T)$ continues to grow in time, with a concomitant increase in t_{co}, and as Eq. (7) will show below, T_f will approach T_g as in Fig. 2.

III. CORRELATION LENGTH GROWTH AND ACTIVATION ENERGY

Spin-glass dynamics depend upon the cooling protocol to reach the final measurement temperature T_m. For example, the dynamics will be different if the sample is quenched from an initial temperature above the spin-glass transition temperature T_g to the measurement temperature T_m compared to a temperature change from an initial temperature below

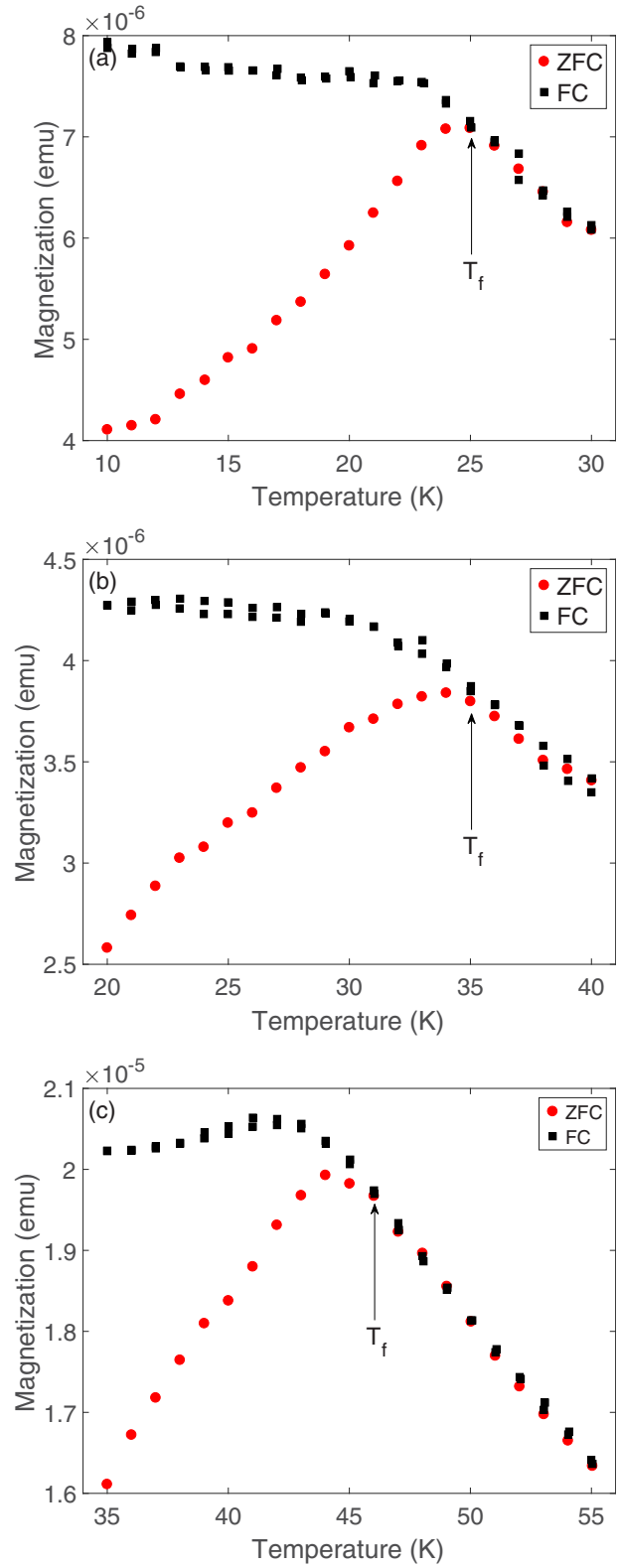

FIG. 1. Freezing-temperature measurements in a magnetic field of 40 G: (a) a 4.5-nm CuMn thin film exhibits a freezing temperature near 25 K, (b) a 9-nm CuMn thin film exhibits a freezing temperature near 35 K, and (c) a 20-nm CuMn thin film exhibits a freezing temperature near 46 K.

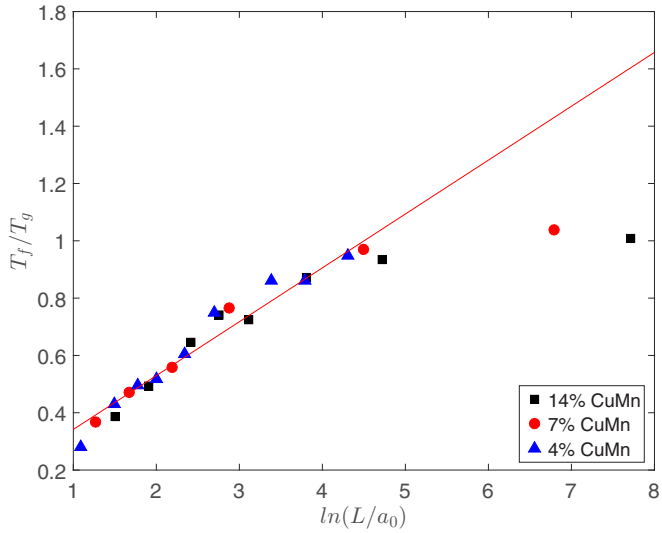

FIG. 2. The freezing temperatures T_f from Table VII of Ref. [21] for different Mn concentrations plotted against $\ln(\mathcal{L}/a_0)$. The straight line is a best fit to the data for films up to and including $\mathcal{L}/a_0 \leqslant 5$. The two points omitted are for film thicknesses of 1000 nm for CuMn of 14 at. %, and 500 nm for CuMn of 7 at. %. These two films are sufficiently thick that $T_f \sim T_g$.

T_g to T_m. This was the essence of an analysis of previous experimental data [22,23] in Ref. [24]. For the data presented here, the measurements of the dynamics at different T_m were all initiated from temperatures $T > T_g$, so that the initial state was always in the paramagnetic temperature regime.

The spin-glass state grows in size from nucleation as a function of time t with the size scale of the spin-glass correlation length $\xi(t,T)$. The growth of $\xi(t,T)$ differs in the two approaches discussed in the Introduction. For power-law dynamics [25–29],

$$\xi(t,T) = c_1 a_0 \left(\frac{t}{\tau_0}\right)^{c_2(T/T_g)}, \tag{1}$$

where a_0 is the average distance between magnetic moments and c_1 and c_2 are constants determined from our experimental data with values of 1.448 and 0.104, respectively (see below). These values are to be compared with theoretical estimates [25–29] that predict c_1 of order unity and c_2 lying between 0.104 and 0.169.

The largest barrier height separating free-energy states is a function of $\xi(t,T)$ [22] and saturates at a maximum value when $\xi(t_{\rm co},T) = \mathcal{L}$. Because the number of states increases exponentially with increasing $\xi(t,T)$, the dynamics are controlled by the largest barrier $\Delta_{\rm max}(\mathcal{L})$. Its value is determined using the equation [16]

$$\frac{\Delta_{\rm max}(\mathcal{L})}{k_B T_g} = \frac{1}{c_2}\left[\ln\left(\frac{\mathcal{L}}{a_0}\right) - \ln c_1\right]. \tag{2}$$

The maximum barrier height controls the dynamics through the usual Arrhenius law,

$$\frac{1}{\tau} = \frac{1}{\tau_0} e^{-\Delta_{\rm max}(\mathcal{L})/k_B T}. \tag{3}$$

Considering next activated dynamics [8–12], the correlation length grows as

$$\xi(t,T) = \alpha a_0 \left[\left(\frac{T}{T_g}\right)\ln\left(\frac{t}{\tau_0}\right)\right]^{1/\psi}, \tag{4}$$

where α is of order unity and ψ is a critical exponent. Experiments [30–32] and simulations [33,34] find values of ψ between 0.65 and 1.1, with most values close to unity. The spin-glass dynamics obey Eq. (3), with

$$\frac{\Delta_{\rm max}(\mathcal{L})}{k_B T_g} = \left(\frac{\mathcal{L}}{\alpha a_0}\right)^{\psi}. \tag{5}$$

The two relationships for the dependence of $\Delta_{\rm max}(\mathcal{L})$ on $\mathcal{L}$, Eqs. (2) and (5), have different dependences on $\mathcal{L}$. As a consequence of these differences, the spread in observed values of $\Delta_{\rm max}(\mathcal{L})$ as a function of length scale $\mathcal{L}$ will be less for power-law dynamics (varying as $\ln \mathcal{L}$) compared to activated law dynamics (varying as a power of $\mathcal{L}$). Our measured values of $\Delta_{\rm max}(\mathcal{L})$ for $\mathcal{L} = 4.5$, 9, and 20 nm will be compared to these predictions.

IV. CuMn MULTILAYER PREPARATION AND MEASUREMENT PROTOCOLS

The CuMn/Cu multilayer samples consisted of 40 bilayers of either 4.5, 9.0, or 20 nm of CuMn and 60 nm of Cu. The multilayer samples were dc sputtered onto 99.99% Cu foil at an argon pressure of 2 mTorr. Two different 99.999% CuMn targets were utilized (a set of 4.5-, 9.0-, and 20-nm CuMn multilayers from each) with nominal Mn concentrations of 13.5 at. %. The Cu target was 99.999% Cu. Two 1-μm-thick CuMn films were grown, one from each target, and magnetometry measurements on these "bulk" samples yielded similar magnetic properties with a spin-glass temperature T_g of 54 ± 1 K for one target and 52 ± 1 K for the other. For simplicity, we shall take $T_g = 53$ K in what follows. Using the extrapolation of Refs. [35,36], this translates to a thin-film Mn concentration of $\approx$11.7 at. %.

The experimental data on the multilayers were obtained in two laboratories. The measurements at The University of Texas at Austin were performed on a Quantum Design superconducting quantum interference device (SQUID) magnetometer, while those at Indiana University of Pennsylvania were performed on a home-built SQUID magnetometer. The former measured the time-dependent zero-field-cooled and field -cooled magnetizations, $M_{\rm ZFC}(t,T)$ and $M_{\rm FC}(t,T)$, while the latter measured the thermoremanent magnetization $M_{\rm TRM}(t,T)$. In both laboratories, the CuMn mesoscale multilayer samples were quenched from a temperature of $\approx$90 K to a measurement temperature $T_m < T_g$ at a rate of $\sim$10 K/min.

The Indiana University of Pennsylvania apparatus is operated in a stationary mode, as opposed to relying on motion through pickup coils, reducing mechanical noise. In addition, the system has two SQUIDs, with the sample located in one set of gradiometer coils measured by SQUID A, while a second gradiometer set measured by SQUID B determined the background electromagnetic noise as well as other possible spurious fluctuations. These artifact contributions to our signal

were then removed from the sample signal by subtracting the response of SQUID B from that of SQUID A.

The measurements of the two systems are complementary, as shown by the extended principle of superposition [37],

$$M_{\rm ZFC}(t,T) + M_{\rm TRM}(t,T) = M_{\rm FC}(t,T). \tag{6}$$

In our experiments, like those in Ref. [37], "$M_{\rm ZFC}(t,T)$ yields a direct measure of the response function." The field-cooled magnetization $M_{\rm FC}(t,T)$ is time dependent in both, so that the time dependence of the irreversible magnetization $M_{\rm TRM}(t,T)$ from a zero-field-cooled experiment is the *difference* between the two time-dependent quantities, $M_{\rm FC}(t,T) - M_{\rm ZFC}(t,T)$. Thus, two independent measurements must be made to obtain the time dependence of the irreversible magnetization. For $t \geqslant t_{\rm co}$, the slope of the logarithm of the irreversible magnetization as a function of t generates the activation energy $\Delta_{\rm max}(\mathcal{L})$.

For the data in Fig. 1, the sample was quenched from an initial high temperature T_h well above the bulk spin-glass temperature T_g to the beginning measurement temperature T_m; then a magnetic field of 40 G was applied, and $M_{\rm ZFC}(t,T)$ was measured as a function of increasing temperature to the value T_h. The magnetization was then measured as the sample was cooled from T_h to T_m, with the magnetic field remaining constant at 40 G, generating $M_{\rm FC}(t,T)$.

At first glance, this protocol may seem reasonable, but it is insufficient for dynamical measurements for the following reason. When the magnetic field is first applied, the spin-glass states with energy barriers $\Delta(t,T) \leqslant E_{\rm Z}$, where $E_{\rm Z}$ is the change in Zeeman energy, are quenched. This allows instantaneous transitions of those states in the initial $M = 0$ manifold to the new free-energy ground-state manifold with $M = M_{\rm FC}(t,T)$.

Because $M_{\rm FC}(t,T)$ changes with time, when the magnetic field is applied, some (small) magnetization arises from states that transition before magnetization measurements can be made. This time-varying magnetization must be subtracted from the *measured* time-dependent difference in magnetizations, $M_{\rm FC}(t,T) - M_{\rm ZFC}(t,T)$, to obtain the true measured irreversible magnetization. The manner in which this is accomplished is to measure the ratio $M_{\rm ZFC}(t,T)/M_{\rm FC}(t,T) \equiv \alpha(t)$ as a function of time t until it reaches a final constant value α_f to within measurement error bars. For $\alpha_f = 1$, this would signify that $M_{\rm ZFC}(t,T)$ has reached the field-cooled value for the magnetization $M_{\rm FC}(t,T)$. However, because of the time interval for which the measurement of $M_{\rm ZFC}(t,T)$ is "blind," $\alpha_f < 1$, requiring a subtraction of the contribution to $M_{\rm FC}(t,T)$ that occurred during that time interval. This is accomplished by subtracting an amount $\epsilon = 1 - \alpha_f$ from the measured $M_{\rm FC}(t,T)$. The irreversible magnetization, $(1-\epsilon)M_{\rm FC}(t,T) - M_{\rm ZFC}(t,T)$, then approaches zero in the long-time limit. Typically, ϵ is found to be small, on the order of 0.005. Values of $1-\epsilon$ are included in the caption for Fig. 3.

The time dependence of the field-cooled magnetization $M_{\rm FC}(t,T)$ is much stronger for mesoscale spin glasses than for bulk because of the finite number of magnetic moments at the mesoscale, giving rise to "glassy" dynamics. Given that the average distance between Mn spins at our sample concentration of 11.7 at. % is 0.523 nm, we find for $\xi(t \geqslant t_{\rm co}, T) = \mathcal{L} = 4.5$, 9, and 20 nm a total of ≈334, 2668, and 29 281 moments in the correlation volume, respectively.

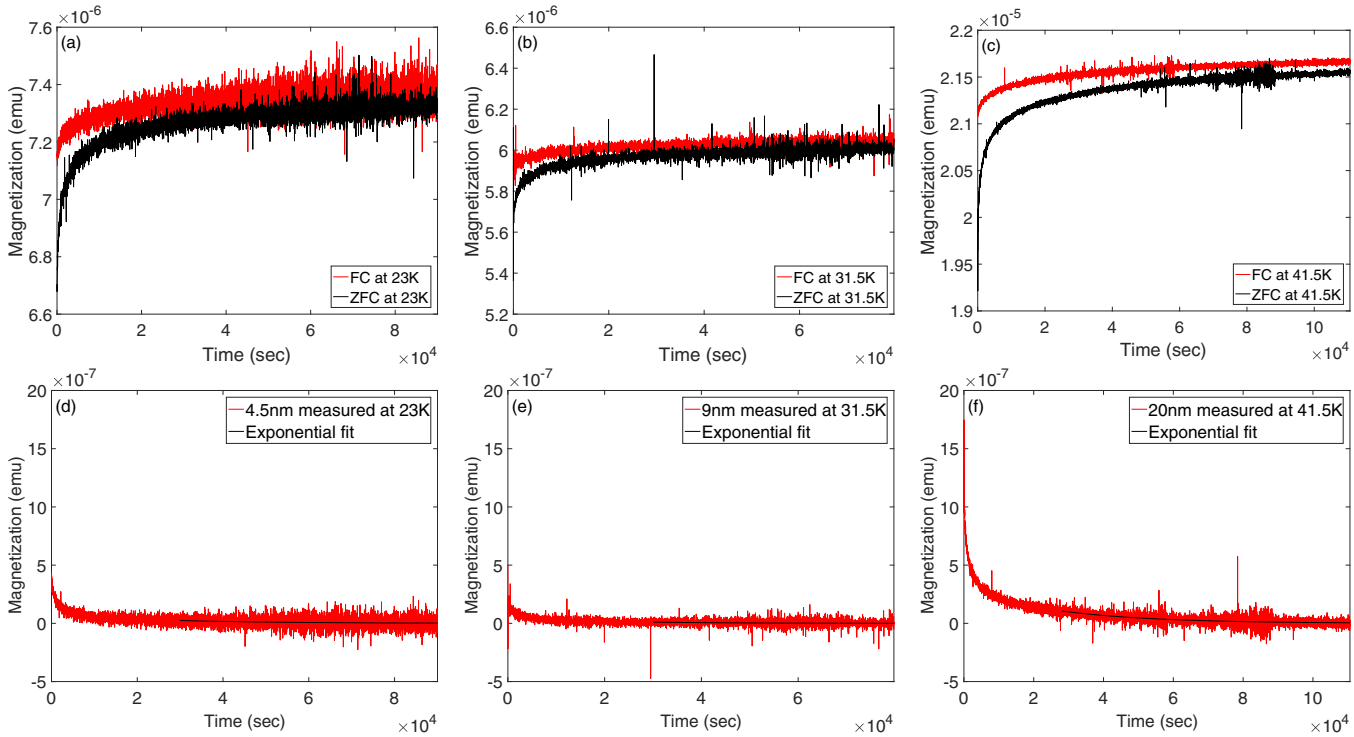

FIG. 3. (a)–(c) The measured magnetizations, $M_{\rm FC}(t,T)$ and $M_{\rm ZFC}(t,T)$, plotted against time for the three CuMn multilayer thin films at a representative temperature. (d)–(f) $(1-\epsilon)M_{\rm FC}(t,T) - M_{\rm ZFC}(t,T)$ and its exponential fit to activated dynamics. (a) and (d) A 4.5-nm film at 23 K, $1-\epsilon = 0.994$, (b) and (e) 9.0-nm film at 31.5 K, $1-\epsilon = 0.994$, and (c) and (f) 20-nm film at 41.5 K, $1-\epsilon = 0.995$.

The consequences will be shown in the experimental results in the next section and in the summary and conclusion (Sec. VII).

V. EXPERIMENTAL RESULTS

The time-dependent $M_{\rm ZFC}(t,T)$ and $M_{\rm FC}(t,T)$ of the multilayer samples were measured in a commercial Quantum Design SQUID magnetometer. As previously explained, because $M_{\rm FC}(t,T)$ is time dependent, it was necessary to perform time-dependent measurements for both $M_{\rm ZFC}(t,T)$ and $M_{\rm FC}(t,T)$ with exactly the same time and temperature protocol as outlined in Sec. IV. Specifically, a magnetic field of 40 G was applied 135 s after reaching T_m, and the temperature was stabilized; the magnetization was then measured as a function of time until well beyond the crossover time $t_{\rm co}$. Then the temperature was increased back to ~90 K with the magnetic field held constant and then quenched at the same rate as before to the same T_m. The $M_{\rm FC}(t,T)$ was then measured for the same time period as the $M_{\rm ZFC}(t,T)$. The time-dependent values of $M_{\rm ZFC}(t,T)$ and $M_{\rm FC}(t,T)$ are displayed in Fig. 3 for each of the three CuMn thin-film thicknesses $\mathcal{L}$ at a respective representative temperature.

Figures 3(a)–3(c) are representative of $M_{\rm FC}(t,T)$ and $M_{\rm ZFC}(t,T)$ for the three thicknesses. The difference, $(1-\epsilon)M_{\rm FC}(t,T) - M_{\rm ZFC}(t,T)$ as derived in Sec. IV, is the time and temperature dependence of the irreversible component of the spin-glass magnetization and is displayed in Figs. 3(d)–3(f). From Eq. (1), there exists a time $t_{\rm co}$ when $\xi(t,T) = \mathcal{L}$. For times longer than $t_{\rm co}$, the irreversible magnetization dynamics are activated [2], with activation energy $\Delta_{\rm max}(\mathcal{L})$ given by Eq. (2); the two are related through Eq. (3). Hence, the time $t = t_{\rm co}$, when $(1-\epsilon)M_{\rm FC}(t_{\rm co},T) - M_{\rm ZFC}(t_{\rm co},T)$ crosses over to activated behavior, is related to $\Delta_{\rm max}(\mathcal{L})$ through Eqs. (1) and (2), as well as Eqs. (4) and (5), and can be determined from the slope of $\ln[(1-\epsilon)M_{\rm FC}(t,T) - M_{\rm ZFC}(t,T)]$ vs t for $t \geqslant t_{\rm co}$. From both Eqs. (2) and (5), $\Delta_{\rm max}(\mathcal{L})$ should be independent of the measurement temperature T_m. Most important is the determination of $\Delta_{\rm max}(\mathcal{L})$ as a function of the different film thicknesses $\mathcal{L}$ because of the different proportionality of $\Delta_{\rm max}(\mathcal{L})$ to $\mathcal{L}$ between Eqs. (2) and (5).

A representative fitting of an exponential decay curve to $(1-\epsilon)M_{\rm FC}(t,T) - M_{\rm ZFC}(t,T)$ for times longer than $t_{\rm co}$ is displayed in Figs. 3(d)–3(f) for each of the three film thicknesses. Table I lists the values of $\Delta_{\rm max}(\mathcal{L})$ at three different measurement temperatures for each film thickness. As can be seen, $\Delta_{\rm max}(\mathcal{L})$ is *independent* of the measurement temperature within experimental error and is only a function of film thickness $\mathcal{L}$, as postulated in Sec. III.

TABLE I. $\Delta_{\rm max}(\mathcal{L})/k_B$ extracted at different temperatures for each multilayer CuMn thin film.

$\mathcal{L}$ (nm)	T_f (K)	T_m (K)	$\Delta_{\rm max}(\mathcal{L})/k_B$ (K)
4.5	25	22.5	907 ± 2
		23	910 ± 7
		23.5	904 ± 2
9	35	31	1243 ± 8
		31.5	1243 ± 13
		32	1252 ± 10
20	46	41	1648 ± 4
		41.5	1650 ± 2
		42	1652 ± 8

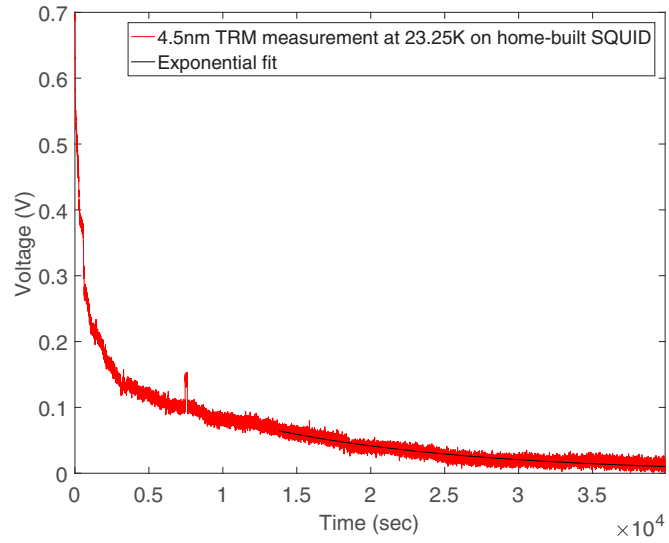

FIG. 4. The $M_{\rm TRM}(t, T = 23.25\ {\rm K})$ SQUID voltage plotted against time t. For $t \geqslant t_{\rm co} \approx 1.4 \times 10^4$ s, $M_{\rm TRM}(t, T = 23.25)$ K displays activated behavior with $\Delta_{\rm max}(\mathcal{L} = 4.5\ {\rm nm}) = 909 \pm 5$ K.

Taking the mean values for $\Delta_{\rm max}(\mathcal{L})/k_B$ from Table I, we arrive at $\Delta_{\rm max}(4.5\,{\rm nm})/k_B \simeq 907$ K, $\Delta_{\rm max}(9.0\,{\rm nm})/k_B \simeq 1246$ K, and $\Delta_{\rm max}(20.0\,{\rm nm})/k_B \simeq 1650$ K.

An independent check on the above analysis was performed on the 4.5-nm multilayer sample from thermoremanent magnetization data $M_{\rm TRM}(t,T)$ measured over a broad temperature range in a magnetic field of 20 G. A representative plot of $M_{\rm TRM}(t,T)$ vs time t is displayed in Fig. 4 at $T_m = 23.25$ K. The crossover time for this temperature and film thickness (4.5 nm) is $t_{\rm co} \approx 1.4 \times 10^4$ s (see also the data exhibited in Fig. 2), so that the fitted slope is well within the activated dynamical range. The activation energy extracted from Fig. 4 is $\Delta_{\rm max}(4.5\,{\rm nm})/k_B = 909 \pm 5$ K, in the middle of the values reported in Table I. The agreement of this independent measurement of $\Delta_{\rm max}(\mathcal{L})$ for $\mathcal{L} = 4.5$ nm from $M_{\rm TRM}(t,T)$ measurements, complementary to those reported for $M_{\rm ZFC}(t,T)$ in Table I, gives confidence in the rather complex analysis required for the latter.

Measurements of $M_{\rm ZFC}(t,T)$ and $M_{\rm FC}(t,T)$ display a separation at a temperature that we designate as the "freezing temperature" $T_f(\mathcal{L})$ [21], as discussed earlier. The values of $T_f(\mathcal{L})$ are film thickness dependent, as illustrated in Fig. 1 for each of the thin-film thicknesses $\mathcal{L}$. The values extracted from Fig. 1 are $T_f(4.5\,{\rm nm}) \approx 25 \pm 1$ K, $T_f(9.0\,{\rm nm}) \approx 35 \pm 1$ K, and $T_f(20\,{\rm nm}) \approx 46 \pm 1$ K and are listed in Table I.

VI. ANALYSIS AND COMPARISON WITH THEORIES

The value of $T_f(\mathcal{L})$ is a function of the time scale of the experiment, as was first observed for the "knee" in the $M_{\rm FC}(T)$ data in Ref. [22]. The time dependence of $T_f(\mathcal{L})$ is reminiscent of the conventional glass transition [38], which "is not a thermodynamic transition at all, since T_g is only empirically

defined as the temperature below which the material has become too viscous to flow on a 'reasonable' time scale."

For power-law dynamics, Eq. (2) relates the dominating maximum barrier height $\Delta_{\max}(\mathcal{L})$ to $\mathcal{L}$ when the correlation length $\xi(t,T)$ has reached the film thickness $\mathcal{L}$ at $t_{\rm co}$. This sets the time scale for our experiments $t_{\rm exp}$ through Eq. (3) and fixes T_f. Solving Eq. (3) for $\Delta_{\max}(\mathcal{L})$ when $\tau = t_{\rm co}$ and substituting this into Eq. (2) yield

$$\frac{T_f}{T_g} c_2 \ln\left(\frac{t_{\rm co}}{\tau_0}\right) + \ln\, c_1 = \ln\left(\frac{\mathcal{L}}{a_0}\right). \tag{7}$$

We extract T_f from the experimental data as the temperature at which the irreversible magnetization first appears approaching T_g from above, that is, when $M_{\rm ZFC}(t,T_f) = M_{\rm FC}(t,T)$. Because $M_{\rm FC}$ is time dependent, $M_{\rm ZFC}(t,T)$ is "chasing" a moving target, $(1-\epsilon)M_{\rm FC}(t,T)$. In general the time dependence of $M_{\rm ZFC}(t,T)$ is much faster than $(1-\epsilon)M_{\rm FC}(t,T)$, so that one can consider the end of irreversibility to take place when $M_{\rm ZFC}(t,T)$ has reached $(1-\epsilon)M_{\rm FC}(t,T)$. For mesoscopic spin-glass films, the time scale of the growth of $M_{\rm ZFC}(t,T)$ is roughly $\tau_0 \exp(\Delta_{\max}/k_B T)$. Hence, $\Delta_{\max}$ sets the time scale for irreversibility to vanish, or, concomitantly, for the freezing temperature T_f. Thus, for a given time scale of the experiment $t_{\rm exp}$, the freezing temperature is set by $t_{\rm exp} \sim \tau_o \exp(\Delta_{\max}/k_B T_f)$, similar in concept to the conventional glass transition. But from Eq. (2), $\Delta_{\max} \propto \ln \mathcal{L}$. This scaling relationship of $T_f \propto \ln \mathcal{L}$ for reasonably constant $t_{\rm exp}$ is the basis for the Kenning effect [21].

For activated dynamics, Fisher and Huse [8] found a power-law relationship between $T_f(\mathcal{L})/T_g$ and $\mathcal{L}$ given by

$$\frac{T_f(\mathcal{L})}{T_g}\left[\ln\left(\frac{\tau(\mathcal{L})}{\tau_0}\right)\right]^{1/(1+\nu_2\psi_2)} = \left(\frac{\mathcal{L}}{a_0}\right)^{(\psi_3+\psi_2\nu_2\theta_3)/(1+\psi_2\nu_2)}, \tag{8}$$

where the subscripts denote the dimensionality of the parameters. To evaluate this equation, we need values for ψ_2, ψ_3, ν_2, and θ_3. From Refs. [30–33], $\psi_2 \simeq 1.0$, and Ref. [39] found $\nu_2 \simeq 3.45$, leading to the product for $\psi_2\nu_2 \simeq 3.45$. This is in contrast to the fitted experimental value $\psi_2\nu_2 = 1.6 \pm 0.2$ from Ref. [22]. The exponent $\theta_3 \approx 0.2$ from Ref. [8]. Putting the theoretically derived numbers together with the experimental value for ψ_2, one finds

$$\left(\frac{T_f(\mathcal{L})}{T_g}\right)^{4.45} \ln\left(\frac{\tau(\mathcal{L})}{\tau_0}\right) = \left(\frac{\mathcal{L}}{a_0}\right)^{(\psi_3+0.69)}. \tag{9}$$

For the 9.0-nm film, $T_f(\mathcal{L})/T_g = 0.66$, so that Eq. (9) becomes

$$\ln\left(\frac{\tau(9.0\,\text{nm})}{\tau_0}\right) = 6.338 \times (17.2)^{(\psi_3+0.69)}. \tag{10}$$

Reference [8] found $\psi_3 \geqslant \theta_3 \approx 0.2$, and even taking the smallest possible value for $\psi_3 = 0.2$ from θ_3 given above yields an impossibly large value for $\tau(9.0\,\text{nm}) \sim 10^{21}$ s. Using the experimental value [20] for $\psi_2\nu_2 = 1.6$ results in

$$\ln\left(\frac{\tau(9.0\,\text{nm})}{\tau_0}\right) = 2.941 \times (17.2)^{(\psi_3+0.32)}. \tag{11}$$

Taking again the smallest possible value for $\psi_3 = 0.2$ yields an impossibly small value for $\tau(9.0\,\text{nm}) \sim 5 \times 10^{-8}$ s. Setting $\tau(9.0\,\text{nm})$ equal to $t_{\rm co}$ for power-law dynamics, $\tau(9.0\,\text{nm}) \approx$ 416 s, would require $\psi_3 = 0.56$, a not unreasonable value. Using this value for ψ_3, one can calculate $\ln[\tau(\mathcal{L})/\tau_0]$ for the other two thicknesses. Using Eq. (8) with $\psi_3 = 0.56$ yields values of $\tau(4.5\,\text{nm}) \sim 2.3 \times 10^7$ s, much longer than we find from our experiments, and of $\tau(20.0\,\text{nm}) \sim 284$ s, which is much shorter. This large spread of times is a consequence of the power-law relation of $\tau(\mathcal{L})$ to $\mathcal{L}$ for activated dynamics as opposed to the logarithmic relation of $\tau(\mathcal{L})$ to $\mathcal{L}$ for power-law dynamics.

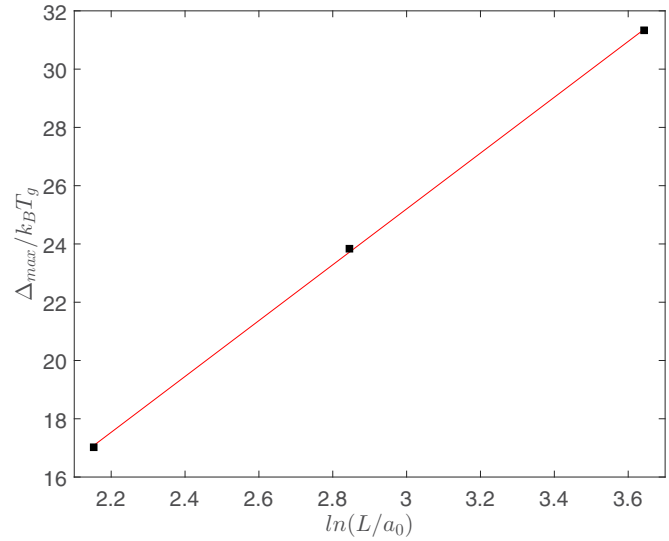

FIG. 5. A plot of the calculated values of $\Delta_{\max}(\mathcal{L})$ as a function of $\ln(\mathcal{L}/a_0)$ using $c_1 = 1.448$ and $c_2 = 0.104$ in Eq. (2). The closeness to the drawn straight line, a requirement of Eq. (2), is an indication of the consistency of fit for power-law dynamics.

In addition to the freezing temperatures, the experimental results of Sec. V also generated the activation energies for the three thin-film thicknesses $\Delta_{\max}(\mathcal{L})$. Repeating from Sec. V, $\Delta_{\max}(4.5\,\text{nm})/k_B = 907$ K, $\Delta_{\max}(9.0\,\text{nm})/k_B = 1246$ K, and $\Delta_{\max}(20.0\,\text{nm})/k_B = 1650$ K. Equations (2) and (5) give values for $\Delta_{\max}(\mathcal{L})$ for power-law dynamics and activated dynamics, respectively.

For power-law dynamics, values for $c_1 = 1.448$ and $c_2 = 0.104$ can be extracted from the values for $\Delta_{\max}(\mathcal{L})$ using Eq. (2). Because we have three thicknesses $\mathcal{L}$, c_1 and c_2 are overdetermined. A best fit results in $c_1 = 1.448$ and $c_2 = 0.104$. Using these values for c_1 and c_2, $\Delta_{\max}(\mathcal{L})$ can in turn be evaluated as a function of $\mathcal{L}$ from Eq. (2). The results are displayed in Fig. 5, where the closeness of the experimental values to the straight line is a display of the consistency of fit for power-law dynamics.

For activated dynamics, one needs the value of the coefficient α in Eq. (5), and that requires a value for the exponent $\psi \equiv \psi_2$ in this case. Using the value $\psi_2 = 1.0$, consistent with Refs. [30–32], and fitting to the measured value for $\Delta_{\max}(9.0\,\text{nm})/k_B = 1246$ K, we find $\alpha = 0.73$ from Eq. (5), close to unity as expected from Refs. [8–12]. Using these values for ψ and α, we can calculate $\Delta_{\max}(\mathcal{L})$ for the other two film thicknesses to test for consistency. We find $\Delta_{\max}(4.5\,\text{nm})/k_B = 623$ K and $\Delta_{\max}(20.0\,\text{nm})/k_B = 2769$ K. They are much smaller and much larger, respectively, than the experimental values.

The spread of values for $\Delta_{\max}(\mathcal{L})$ differs substantially between the two descriptions because of the differing dependences on $\mathcal{L}$. The power-law dynamics proportionality to $\ln(\mathcal{L}/a_0)$ increases much more slowly with increasing $\mathcal{L}/a_0$ than the algebraic proportionality to $(\mathcal{L}/a_0)^{\psi}$ of activated dynamics.

VII. SUMMARY AND CONCLUSIONS

We have presented a systematic study of thin-film spin-glass dynamics as a function of length scale $\mathcal{L}$. As noted in the Introduction, when the spin-glass correlation length $\xi(t,T)$ reaches $\mathcal{L}$, the system crosses over to the dimension $D = 2$. This is below the lower critical dimension of a spin glass ($\approx$2.5), and thus, $\xi(t,T)$ is fixed at $\mathcal{L}$. Varying $\mathcal{L}$ allows measurement of the length-scale dependence of the maximum barrier height $\Delta(\mathcal{L})$ and the (glasslike) freezing temperature $T_f(\mathcal{L})$.

Predictions for the length-scale dependence of both $\Delta(\mathcal{L})$ and $T_f(\mathcal{L})$ were calculated from two competing theories. Quantitative agreement between the experimental data and power-law dynamics for $\xi(t,T)$ is found, while using reasonable values for the parameters in activated dynamics predicts a much greater variation with $\mathcal{L}$ than found experimentally.

The thicknesses explored in these experiments contain a modest number of magnetic spins N, which is sufficiently small that direct comparisons with simulations are possible. As discussed in Sec. IV, the dynamical measurements reported here are for $N \approx 334$ spins ($\mathcal{L} = 4.5$ nm), $N \approx 2668$ spins ($\mathcal{L} = 9.0$ nm), and $N \approx 29\,281$ spins ($\mathcal{L} = 20.0$ nm). Simulations using the Janus special-purpose computer have reported equilibrium properties for millions of Ising spins [40]. It seems possible that simulations of nonequilibrium dynamical properties of Ising spins are possible for numbers of spins comparable to those contributing in our experiments [41].

Finally, these experiments have established the dynamical properties of spin glasses as a function of length scale for fixed temperatures and magnetic fields. The issue of dynamics associated with changes in these parameters has yet to be explored. To quote Ref. [42], "An experimental measurement of TC [temperature chaos] is still missing" (but see Ref. [3], where temperature chaos is reported for a mesoscopic GeMn amorphous spin glass). Now that the dynamical properties of spin glasses at fixed temperature are in hand, systematic exploration of temperature changes under conditions leading to temperature chaos in conventional spin glasses (e.g., CuMn) should be possible. Further, a similar opportunity is present for magnetic field chaos, an effect that has been explored theoretically much less than temperature chaos [43]. Spin glasses at the mesoscale can serve as a laboratory for further explorations under controlled conditions.

ACKNOWLEDGMENTS

It is a pleasure to acknowledge many helpful exchanges with Dr. V. Martin-Mayor. This work was supported by the U.S. Department of Energy, Office of Science, Office of Basic Energy Sciences, Award No. DE-SC0013599.

[1] Basic Energy Sciences Advisory Committee Subcommittee on Mesoscale Science, *From Quanta to the Continuum: Opportunities for Mesoscale Science* (U.S. Department of Energy, Washington, DC, 2012), https://science.energy.gov/~/media/bes/pdf/reports/files/From_Quanta_to_the_Continuum_rpt.pdf.

[2] S. Guchhait and R. Orbach, Direct Dynamical Evidence for the Spin Glass Lower Critical Dimension $2 < d_\ell < 3$, Phys. Rev. Lett. **112**, 126401 (2014).

[3] S. Guchhait and R. L. Orbach, Temperature chaos in a Ge:Mn thin-film spin glass, Phys. Rev. B **92**, 214418 (2015).

[4] S. Franz, G. Parisi, and M. A. Virasoro, Interfaces and lower critical dimension in a spin-glass model, J. Phys. I **4**, 1657 (1994).

[5] L. W. Lee and A. P. Young, Large-scale monte carlo simulations of the isotropic three-dimensional heisenberg spin glass, Phys. Rev. B **76**, 024405 (2007).

[6] G. Parisi, Towards a mean field-theory for spin-glasses, Phys. Lett. A **73**, 203 (1979); Infinite Number of Order Parameters for Spin-Glasses, Phys. Rev. Lett. **43**, 1754 (1979); A sequence of approximated solutions to the S-K model for spin-glasses, J. Phys. A **13**, L115 (1980).

[7] D. Sherrington and S. Kirkpatrick, Solvable Model of a Spin-Glass, Phys. Rev. Lett. **35**, 1792 (1975).

[8] D. S. Fisher and D. A. Huse, Ordered Phase of Short-Range Ising Spin-Glass, Phys. Rev. Lett. **56**, 1601 (1986).

[9] D. A. Huse and D. S. Fisher, Pure states in spin glasses, J. Phys. A **20**, L997 (1987).

[10] D. S. Fisher and D. A. Huse, Static and dynamic behavior of spin-glass films, Phys. Rev. B **36**, 8937 (1987).

[11] D. S. Fisher and D. A. Huse, Nonequilibrium dynamics of spin glasses, Phys. Rev. B **38**, 373 (1988).

[12] D. S. Fisher and D. A. Huse, Equilibrium behavior of the spin-glass ordered phase, Phys. Rev. B **38**, 386 (1988).

[13] A. J. Bray and M. A. Moore, Critical behavior of the three-dimensional Ising spin-glass, Phys. Rev. B **31**, 631 (1985).

[14] W. L. McMillan, Domain-wall renormalization-group study of the three-dimensional random Ising model at finite temperature, Phys. Rev. B **31**, 340 (1985).

[15] K. Jonason, E. Vincent, J. Hammann, J. P. Bouchaud, and P. Nordblad, Memory and Chaos Effects in Spin Glasses, Phys. Rev. Lett. **81**, 3243 (1998).

[16] Y. G. Joh, R. Orbach, G. G. Wood, J. Hammann, and E. Vincent, Extraction of the Spin Glass Correlation Length, Phys. Rev. Lett. **82**, 438 (1999).

[17] K. Jonason, P. Nordblad, E. Vincent, J. Hammann, and J.-P. Bouchaud, Memory interference effects in spin glasses, Eur. Phys. J. B **13**, 99 (2000).

[18] J.-P. Bouchaud, V. Dupuis, J. Hammann, and E. Vincent, Separation of time and length scales in spin glasses: Temperature as a microscope, Phys. Rev. B **65**, 024439 (2001).

[19] J. R. L. de Almeida and D. J. Thouless, Stability of sherrington-kirkpatrick solution of a spin glass model, J. Phys. A **11**, 983 (1978).

[20] J. A. Cowen, G. G. Kenning, and J. M. Slaughter, Magnetic susceptibility and magnetic resonance of a composition-modulated spin glass, J. Appl. Phys. **61**, 4080 (1987); G. G. Kenning, J. M. Slaughter, and J. A. Cowen, Finite-Size Effects in a CuMn Spin-Glass, Phys. Rev. Lett. **59**, 2596 (1987); J. A. Cowen, G. G. Kenning, and J. Bass, Finite size effects in a metallic spin glass, J. Appl. Phys. **64**, 5781 (1988).

[21] G. G. Kenning, J. Bass, W. P. Pratt, Jr., D. Leslie-Pelecky, L. Hoines, W. Leach, M. Wilson, R. Stubi, and J. A. Cowen, Finite-size effects in Cu-Mn spin glasses, Phys. Rev. B **42**, 2393 (1990).

[22] L. Sandlund, P. Granberg, L. Lundgren, P. Nordblad, P. Svedlindh, J. A. Cowen, and G. G. Kenning, Dynamics of Cu-Mn spin-glass films, Phys. Rev. B **40**, 869(R) (1989).

[23] P. Granberg, P. Nordblad, P. Svedlindh, L. Lundgren, R. Stubi, G. G. Kenning, D. L. Leslie-Pelecky, J. Bass, and J. Cowen, Dimensionality crossover in CuMn spin-glass films, J. Appl. Phys. **67**, 5252 (1990).

[24] S. Guchhait, G. G. Kenning, R. L. Orbach, and G. F. Rodriguez, Spin glass dynamics at the mesoscale, Phys. Rev. B **91**, 014434 (2015).

[25] E. Marinari, G. Parisi, J. Ruiz-Lorenzo, and F. Ritort, Numerical Evidence for Spontaneously Broken Symmetry in 3D Spin Glasses, Phys. Rev. Lett. **76**, 843 (1996).

[26] J. Kisker, L. Santen, M. Schreckenberg, and H. Rieger, Off-equilibrium dynamics in finite-dimensional spin-glass models, Phys. Rev. B **53**, 6418 (1996).

[27] J.-O. Andersson and P. Sibani, Domain growth and thermal relaxation in spin glasses, Phys. A (Amsterdam, Neth.) **229**, 259 (1996).

[28] F. Belletti *et al.*, Nonequilibrium Spin-Glass Dynamics from Picoseconds to a Tenth of a Second, Phys. Rev. Lett. **101**, 157201 (2008).

[29] F. Belletti *et al.*, An in-depth view of the microscopic dynamics of Ising spin glasses at fixed temperature, J. Stat. Phys. **135**, 1121 (2009).

[30] A. G. Schins, A. F. M. Arts, and H. W. de Wijn, Domain Growth by Aging in Nonequilibrium Two-Dimensional Random Ising Systems, Phys. Rev. Lett. **70**, 2340 (1993).

[31] C. Dekker, A. F. M. Arts, H. W. de Wijn, A. J. van Duyneveldt, and J. A. Mydosh, Activated Dynamics in the Two-Dimensional Ising Spin-Glass $Rb_2Cu_{1-x}Co_xF_4$, Phys. Rev. Lett. **61**, 1780 (1988).

[32] C. Dekker, A. F. M. Arts, H. W. de Wijn, A. J. van Duyneveldt, and J. A. Mydosh, Activated dynamics in a two-dimensional Ising spin glass: $Rb_2Cu_{1-x}Co_xF_4$, Phys. Rev. B **40**, 11243 (1989).

[33] T. R. Gawron, M. Cieplak, and J. R. Banavar, Scaling of energy barriers in Ising spin-glasses, J. Phys. A **24**, L127 (1991).

[34] H. Rieger, B. Steckemetz, and M. Schreckenberg, Aging and domain growth in the two-dimensional Ising spin glass model, Europhys. Lett. **27**, 485 (1994).

[35] D. C. Vier and S. Schultz, Evidence for Multiple Mechanisms Contributing to the Transition Temperature in Metallic Spin Glasses, Phys. Rev. Lett. **54**, 150 (1985).

[36] U. Larsen, Saturation of ruderman-kittel-kasuya-yosida interaction damping in high-resistivity spin glasses, Phys. Rev. B **33**, 4803 (1986).

[37] P. Nordblad and P. Svedlindh, Experiments on Spin Glasses, in *Spin Glasses and Random Fields*, edited by A. P. Young, Directions in Condensed Matter Physics Vol. 12 (World Scientific, Singapore, 1997), p. 1.

[38] L. Berthier and G. Biroli, Theoretical perspective on the glass transition and amorphous materials, Rev. Mod. Phys. **83**, 587 (2011).

[39] H. G. Katzgraber, L. W. Lee, and A. P. Young, Correlation length of the two-dimensional Ising spin glass with gaussian interactions, Phys. Rev. B **70**, 014417 (2004).

[40] M. Baity-Jesi *et al.*, Janus II: A new generation application-driven computer for spin-system simulations, Comput. Phys. Commun. **185**, 550 (2014).

[41] M. Baity-Jesi *et al.* (Janus Collaboration) (unpublished).

[42] L. A. Fernandez, V. Martin-Mayor, G. Parisi, and B. Seoane, Temperature chaos in 3D Ising spin glasses is driven by rare events, Europhys. Lett. **103**, 67003 (2013).

[43] I. Kondor, On chaos in spin glasses, J. Phys. A **22**, L163 (1989).